GEOPHYSICAL RESEARCH LETTERS, VOL. 18, NO. 6, PAGES 1143-1146, JUNE 1991

# 3-D MODELLING OF SEAMOUNT TOPOGRAPHY FROM SATELLITE ALTIMETRY

Nicolas Baudry

Seafloor Imaging Inc., Nouméa, New Caledonia

Stéphane Calmant

ORSTOM, Nouméa, New Caledonia

Abstract. We develop a complete set of algorithms to perform 3D modelling of seamount bathymery from satellite altimetry. The first stage of the data processing consists in gridding the geoid: to account for the long wavelength errors geoid heights are first bias-adjusted at cross-overs. Then a collocation on a regular grid is performed, accounting for the altimeter errors. In a second stage, geoid heights are converted into bathymetry. No simplifying assumption on the shape and location of the bathymetry highs is necessary. Bathymetric uncertainties due to the data sampling and the parameters of the mechanical and crustal models are evaluated.

## Introduction

Global and regional maps of the gravity field over the world's oceans derived from satellite altimetry are now an efficient tool for the identification of seafloor and crustal features (Bostrom, 1989). In oceanic basins, these maps have lead to spectacular indirect views of the seafloor with a spatial resolution of about 20 to 50km (Haxby et al., 1983; Sandwell et al., 1990). In this paper, we describe a set of algorithms to model seamount bathymetry from Geos-3, Seasat and Geosat satellite altimetry. These algorithms are designed to be used in oceanic areas where few or no direct bathymetric measurements are available, such as the South Pacific ocean. We show that satellite altimetry, combined with elementary geophysical knowledge of the prospected area, provide sufficient information for an accurate and reliable seafloor modelling over seamounts.

Figure 1 shows an image of the residual high-pass filtered geoid over the volcanic chains of French Polynesia (South Central Pacific). At such short wavelengths, there is a strong correlation between the residual geoid and the seafloor bathymetry. The detection of new seamounts in the residual geoid is easy because of the typical signature of seamounts (sub-circular positive highs). On this image, the signature of about 50 uncharted seamounts can be identified.

Once a new seamount has been detected and approximately located, the method to compute seafloor bathymetry described in this paper mainly consists in i) recomputing an accurate gridded geoid over a 1°x1° area centered on the new seamount's approximative location, and ii) inverting this gridded geoid to modelize the seafloor bathymetry and associated accuracy. Geoid and bathymetry are computed onto 0.05°x0.05°grid points.

## Gridding the Geoid

Most of the errors which affect the measuring of the Mean Sea Surface (atmospheric, orbital and oceanic errors) generate constant deviations on the along track values, noticeable as cross-overs discrepancies. Yet, these errors work at too long wavelengths (spatial and temporal domains) to present noticeable along track variations within 1°x1° areas. We then start processing the data by reducing the biases at cross-overs.

Biases corrections. In a first stage, along track biases on the data are globally determined and removed within each separate group of intersecting tracks (Menke, 1984). In a second stage, we correct these heights for the residual biases which may persist between groups. For that, we select a reference group (as the one with most data points) which is used to generate reference values (using the collocation technics described in the following section) at the location of the other data points. Each group-bias is then computed as the mean difference between data and reference values, and data are corrected for these group-biases.

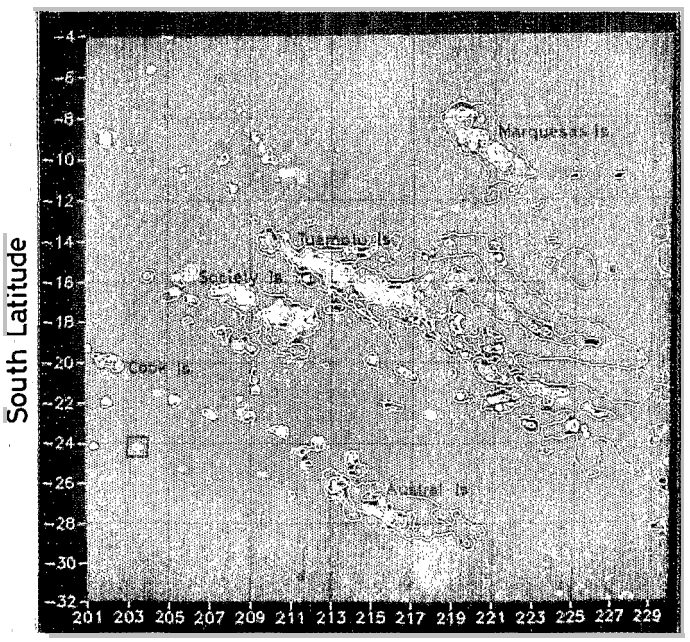


Fig. 1. Image of residual high-pass filtered geoid over the South Central Pacific seamount chains. Prior to filtering, the potential field model GRIM3-L1 up to degree and order 20 was removed from Seasat and Geos-3 altimeter data. Then, profiles were independently high-pass filtered using a 700km cut-off wavelength Butterworth filter. Track spacing varies from a few kilometers to about 50km. After filtering, profiles were interpolated over a 0.1° x 0.1° grid, and a median filter applied to the gridded data. To enhance the signature of volcanic features (islands and seamounts) only the positive residual geoid undulations are displayed, from +0.15m (light blue) to +2m (light yellow). White solid lines show isobath -1000m to -4000m of SYNBAPS bathymetric data base. The 1° x 1° black square shows the location of the seamount modelized in this study.



Paper number 91GL01341
0094-8534/91/91GL-01341

Collocation. Interpolated values of any discretized function result from both samples and interpolator. A simple way for the interpolated values to only contain the information of the sampled quantity is to use this very signal to build the interpolator. In collocation, the predicted values are linear combinaisons of the samples, with weighting coefficients calculated from the correlation between the prediction and sampling places. If measurement errors are taken into account, the general expression for the interpolated geoid heights $n(\mathbf{r})$ at grid coordinates $\mathbf{r}$ is (Moritz, 1978; Tarantola, 1987):

$$n(\mathbf{r}) = n_0(\mathbf{r}) + C^t_{nn}(\mathbf{s}',\mathbf{r})\,(C_{nn}(\mathbf{s}',\mathbf{s}) + \mathcal{E}(\mathbf{s}',\mathbf{s}))^{-1}\, n_r(\mathbf{s}) \quad (1)$$

$n_0(\mathbf{r})$ is the vector formed by a-priori values of $n(\mathbf{r})$. $n_r(\mathbf{s})$ are residual values at the sample locations ($n_r(\mathbf{s}) = n(\mathbf{s}) - n_0(\mathbf{s})$, $n(\mathbf{s})$ and $n_0(\mathbf{s})$ being the data and a-priori values). $C^t_{nn}(\mathbf{s}',\mathbf{r})$ is the transpose of matrix $C_{nn}(\mathbf{s}',\mathbf{r})$, the a-priori covariance between the samples at $\mathbf{s}'$ and the grid points at $\mathbf{r}$. $C_{nn}(\mathbf{s}',\mathbf{s})$ contains the covariance of the samples with themselves. $\mathcal{E}$ is the sum of the spatial and time error covariances between samples (here restricted to the altimeter noise, $\mathcal{E}(\mathbf{s}',\mathbf{s}) = \sigma_a^2\delta(\mathbf{s}'=\mathbf{s})$, $\delta$ is the Dirac impulse, $\sigma_a$ = 8cm for Geosat, 10cm for Seasat, 30cm for Geos-3). The a-posteriori covariance $C'_{nn}(\mathbf{r}',\mathbf{r})$ is:

$$C'_{nn}(\mathbf{r}',\mathbf{r}) = C_{nn}(\mathbf{r}',\mathbf{r}) - C^t_{nn}(\mathbf{s}',\mathbf{r})\,(C_{nn}(\mathbf{s}',\mathbf{s}) + \mathcal{E}(\mathbf{s}',\mathbf{s}))^{-1}\, C_{nn}(\mathbf{r},\mathbf{s}') \quad (2)$$

with $C_{nn}(\mathbf{r}',\mathbf{r})$ the a-priori covariance related to the reference $n_0(\mathbf{r})$. In gravity problems, an earth potential model is classically used to provide the a-priori information $n_0$ and $C_{nn}$ (Moritz, 1978; Rapp, 1985; Mazzega and Houry, 1989). Since the size of our studied areas is far under the resolution of the current models, we rather use for both $n_0(\mathbf{r})$ and $n_0(\mathbf{s})$ a single value over the area, taken as the minimum of the samples. This choice is induced by an external knowledge - bell shaped- on the shape of the local geoid and provides satisfying final values for unresolved places. Analytical expression of the a-priori auto-covariance of the geoid was determined after trials with a wide variety of formulae (Rapp, 1985; Vassiliou and Schwarz, 1987; Balmino et al., 1979; Moritz, 1978). For seamounts, we retained the isotropic expression:

$$C(x) = \sigma_0^2 / (1 + x/\zeta_{1/2}) \quad (3)$$

with the half-correlation length $\zeta_{1/2} = 0.4°$ and x the spherical distance. This value of $\zeta_{1/2}$ is consistent with those of Rapp (1985) for Louisville Ridge and New England Seamounts. The value at the origin $\sigma_0^2$ ($\sigma_0^2 = C_{nn}(\mathbf{r},\mathbf{r}) = C_{nn}(\mathbf{s},\mathbf{s})$) is taken as the mean squared sum of the residuals $n_r(\mathbf{s})$.

## Seamount topography modelling

Seamount topography modelling from potential field data requires the use of crustal and mechanical models. Bathymetry $b(\mathbf{r})$ is assumed to consist in volcanic edifices loading the oceanic lithosphere, treated as a continuous layer behaving elastically. The crustal model is a standard two-layer oceanic crust model: layer 2 with a thickness $t_2 = 2.5$ km and a density $\rho_{c2} = 2.6$ g.cm$^{-3}$, layer 3 with a thickness $t_3 = 5$ km and a density $\rho_{c3} = 2.9$ g.cm$^{-3}$. Mantle density is $\rho_m = 3.35$ g.cm$^{-3}$. The density of the volcanic load is the density of layer 2. Due to the volcanic loading, the lithosphere undergoes a deformation $w(\mathbf{r})$ which is linearly approximated in the Fourier space by (from Banks et al., 1977):

$$W(\mathbf{k}) = \Phi(\mathbf{k})\, B(\mathbf{k}) \quad (4)$$

where: $$\Phi(\mathbf{k}) = \frac{-g\,(\rho_{c2} - \rho_w)}{D\,|\mathbf{k}|^4 + g(\rho_m - \rho_{c2})}$$

with $\mathbf{k}$ the wavenumber, $B(\mathbf{k})$ the Fourier transform of the bathymetry $b(\mathbf{r})$, and D the flexural rigidity of the elastic plate.

The Fourier transform of the geoid anomaly $N(\mathbf{k}) = \mathbf{Q}(B(\mathbf{k}))$ created by the seafloor bathymetry and the compensating deformation of the crustal density interfaces -layer 2 / layer 3 and Moho discontinuity- is (from Parker, 1972):

$$N(\mathbf{k}) = \frac{2\pi G}{g}\left\{E_1(\mathbf{k})\sum_{n=1}^{\infty}\frac{|\mathbf{k}|^{n-2}}{n!}\,FT[b^n(\mathbf{r})] + E_2(\mathbf{k})\sum_{m=1}^{\infty}\frac{|\mathbf{k}|^{m-2}}{m!}\,FT[w^m(\mathbf{r})]\right\} \quad (5)$$

with:

$$E_1(\mathbf{k}) = (\rho_{c2} - \rho_w)\, e^{-|\mathbf{k}|z_0}$$

$$E_2(\mathbf{k}) = (\rho_{c3} - \rho_{c2})\, e^{-|\mathbf{k}|(z_0+t_2)} + (\rho_m - \rho_{c3})\, e^{-|\mathbf{k}|(z_0+t_2+t_m)}$$

FT denotes the Fourier transform, G is the gravitational constant, g the gravitational acceleration, and $z_0$ the local mean seafloor depth. To determine $b(\mathbf{r})$ from $N(\mathbf{k})$, the Fourier transform of $n(\mathbf{r})$, we use an iterative linearization method. An approximation of (5), linear in $B(\mathbf{k})$ (Ribe and Watts, 1982), combined with (4), is used to compute a starting value $B_0(\mathbf{k})$ of the bathymetry:

$$B_0(\mathbf{k}) = N(\mathbf{k})\, Z(\mathbf{k})^{-1} \quad (6)$$

with: $$Z(\mathbf{k}) = \frac{2\pi G}{g}\,|\mathbf{k}|^{-1}\,\{E_1(\mathbf{k}) + E_2(\mathbf{k})\,\Phi(\mathbf{k})\}$$

Refined values are iteratively obtained using:

$$B_i(\mathbf{k}) = B_{i-1}(\mathbf{k}) + \{N(\mathbf{k}) - \mathbf{Q}(B_{i-1}(\mathbf{k}))\}\, Z(\mathbf{k})^{-1} \quad (7)$$

To avoid the development of short-wavelength instabilities in the computed bathymetry, the transfer function $Z(\mathbf{k})^{-1}$ is set to zero for $\mathbf{k} > \mathbf{k}_{limit}$ with $\mathbf{k}_{limit}$ iteratively increased up to the Nyquist wavenumber. Iterative computation is stopped when a minimum residual difference between $N(\mathbf{k})$ and computed geoid $\mathbf{Q}(B_i(\mathbf{k}))$ is reached. This method is stable and gives rapidly convergent results.

## Application

To illustrate the above algorithms, we have recomputed the bathymetry of a middle-size seamount in the Southern Cook archipelago (South Central Pacific). The geoid signature of this seamount is outlined by the 1°x1° square in Figure 1. This seamount was detected using satellite altimetry and lately Seabeam mapped (Baudry and Diament, 1987). This seamount was chosen because of i) a good coverage in both altimetry (Geosat and Seasat) and Seabeam data (50%), ii) a double cone shape of the seamount, which allows to test the resolution of the bathymetry modelling.

Location of the 1 Hz Geosat (2 cycles of the ERM mission) and Seasat data used to compute the gridded geoid over the seamount, and a contour map of the residual geoid heights are displayed Figure 2.a. Residual heights are

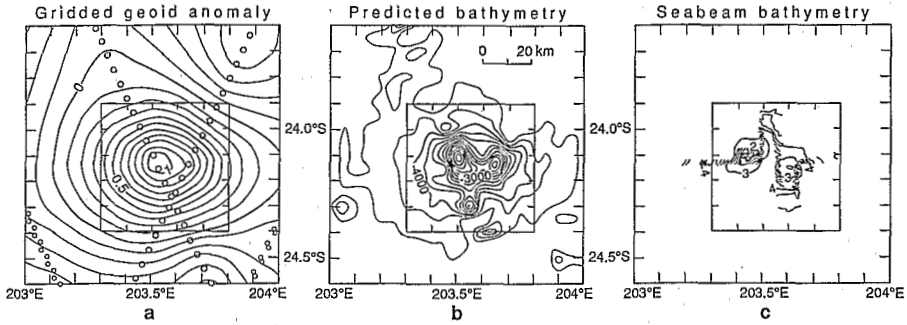


Fig. 2. a. Local variations of the interpolated geoid heights and location of the satellite measurements (1 Htz average) over the studied area. Thick contour circles are for Seasat data and thin ones for Geosat data. Isoline spacing is 0.2 m.
b. Predicted bathymetry of the seamount. Isobaths spacing: 200 m.
c. Seabeam bathymetry of the seamount. Depths in $10^3$ meters. Isobaths spacing: 200m.

obtained by removing a mean plane to the computed geoid. Geos-3 measurements have been discarded because of a very low signal to noise ratio over the studied area. Figure 2.b shows the computed bathymetry of the seamount. The crustal model is the standart oceanic crustal model (see above). The flexural rigidity of the lithosphere is 9 $10^{21}$Nm, as provided by regional experimental studies (Calmant, 1987). Local mean seafloor depth is -4600m, from the global bathymetric data base SYNBAPS. Figure 2.c shows a simplified Seabeam bathymetric map of the seamount which rises from abyssal depths to a minimum depth (west summit) of -1450m. East summit depth is about -2000m.

## Predicted bathymetry accuracy

Bathymetric uncertainties of geoid sampling origin. These specific uncertainties $\sigma_b(\mathbf{r})$ are given by the 0-shift auto-covariance of the bathymetry: $\sigma_b^2(\mathbf{r}) = \mathbf{C}_{bb}(\mathbf{r},\mathbf{r})$. Reducing the expression of $b(\mathbf{r})$ to that of $b_0(\mathbf{r})$ (the inverse Fourier transform of $B_0(\mathbf{k})$, equation (6)), $\mathbf{C}_{bb}$ is given by :

$$\mathbf{C}_{bb}(\mathbf{r},\mathbf{r}') = FT^{-1}\left[ \left| Z(\mathbf{k})^{-1} \right|^2 \; FT\left[ \mathbf{C'}_{nn}(\mathbf{r},\mathbf{r}') \right] \right] \quad (8)$$

where $|Z(\mathbf{k})^{-1}|^2$ is the power spectrum of the linear filter given in (6) and $\mathbf{C'}_{nn}(\mathbf{r},\mathbf{r}')$ is the auto-covariance of the geoid given in (2)). $\sigma_b(\mathbf{r})$ is displayed in Figure 3.a. As expected, low values are found along the satellite tracks and larger values are present far from the samples. These uncertainty computations are scalled by the geoid auto-covariance $\sigma_0^2$. The larger the geoid signal over the studied area, the larger values the geoidal and associated bathymetric uncertainties may take. In the particular case of a flat geoid signal, all the bathymetric uncertainties would be close to zero. Consequently, the larger the extremal value, the more meaningful the low values are, and the important point is that these uncertainties must be analysed first regarding to their dynamic. In Figure 3.a, the lower value is 97m, i.e. the better possible accounting to the signal to noise ratio. This value must be regarded as indicative of a very well resolved restitution since where the restitution is poor, uncertainties as large as 4300m are found.

Bathymetric uncertainties of mechanical and crustal models origin. We will hereafter examine the influence on predicted bathymetry of the two a-priori most sensitive parameters of the mechanical and crustal models, which are the flexural rigidity of the plate and the load-layer 2 density.

Since middle-size seamounts represent short-wavelength bathymetric variations of the seafloor, which are outside the "diagnostic waveband" of the mechanical response of the lithosphere (see Ribe and Watts, 1982), the associated lithospheric flexure is small, whatever the value of the flexural rigidity. Maximum error on the predicted bathymetry due to the uncertainty on D will occur when a seamount with on-ridge compensation (D = $10^{21}$Nm) is assumed to be off-ridge compensated (D = $3.10^{22}$Nm). Figure 3.b shows the differences in predicted bathymetries (computed from the geoid shown Figure 2.a) for such a difference in flexural rigidity. Despite the large variation in the flexural rigidity of

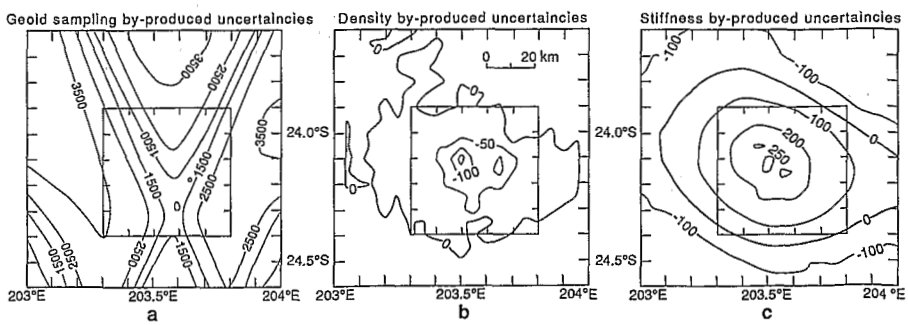


Fig. 3. a. Bathymetry uncertainty of geoidal origin, mainly controlled by the sampling distribution. Values range from 4300 m for poorly resolved grid points, down to less than 500 m for grid points close to satellite tracks: the dynamic is large enough for the low values to be relevant of a good resolution (see text).
b. Bathymetry uncertainty for a 0.1 g.cm$^{-3}$ uncertainty on the load and layer 2 density.
c. Bathymetry uncertainty for a on-ridge/off-ridge uncertainty on the seamount tectonic setting.

the plate, bathymetric differences are quite reasonable (300 m at the center of the load). For middle size seamounts which are not Airy compensated ($D > 10^{21}$Nm), the bathymetry modelling will be relatively unaffected by the value of D.

Local variations of $\rho_{c2}$ (load and layer 2 density), including inhomogeneities in the edifice density, will also lead to errors on the predicted bathymetry. Figure 3.c shows the variations in predicted bathymetry for a 0.1 $g.cm^{-3}$ uncertainty on $\rho_{c2}$. Bathymetric variations range from 0 outside the load (because equation (5) gives bathymetric variations relatively to a mean value which is independant of the crustal model), to 240m at the shallow part of the seamount.

## Discussion and conclusions

Comparison between Figures 2.b and 2.c shows an overall good agreement between computed bathymetry and Seabeam bathymetry. The bulk location of the seamount, marked by the -4000m isobath, is good. Although the two summit shape is resolved, an unavoidable grid-step mislocation (about 6 km) is observed on the summits location. The computed depths of the west and east summits are -1700m and -2300m respectively, corresponding to discrepancies with Seabeam depths of 250m and about 300m. More generally, close to the satellite tracks (where bathymetry uncertainties of geoidal origin are small), bathymetric errors are within the evaluated uncertainties of crustal and mechanical models origin, showing that this set of uncertainties encompasses the major source of errors. The uncertainties of geoidal origin have a dynamic one order greater than those due to uncertainties on the mechanical and crustal models parameters. In one hand, these last uncertainties are small but should not be reduced noticeably since our goal is to map unknown structures, i.e. with limited knowledge on the local geology and tectonic setting. In the other hand, the uncertainties due to the geoid may be considerably reduced (down to less than 500m everywhere) with a denser satellite coverage. It is clear that at that time, the geographical distribution of satellite data is the more limiting factor for seafloor topography restitution. In the early 90's, ERS-1 and Topex/Poseidon data will bring about a dramatic jump for such mapping applications.

## References

Balmino G., C. Brossier, A. Cazenave and F. Nouel, Geoid of the Kerguelen Islands area determined from Geos3 altimeter data, Geophys. J. Res., 84, 3827-3831, 1979.

Banks R.J., R.L. Parker and S.P. Huestis, Isostatic compensation on a continental scale: local versus regional mechanisms, Geophys. J. R. astr. Soc., 51, 431-452, 1977.

Baudry N. and M. Diament, Shipboard confirmation of Seasat bathymetric predictions in the South Central Pacific, in Seamounts, Islands and Atolls, B. Keating, P. Fryer, R. Batiza, and G. Boehlert edit., Geophys. Monograph 43, 115-122, 1987.

Bostrom R.C., Subsurface exploration via satellite: Structure visible in Seasat images of North Sea, Atlantic continental margin, and Australia, Am. Assoc. Petr. Geol. Bull., 73, 1053-1064, 1989.

Calmant S., The elastic thickness of the lithosphere in the Pacific Ocean, Earth and Planet. Sc. Letters, 85, 277-288, 1987.

Haxby W. F., G.D. Karner, J.L. LaBrecque, and J.K. Weissel, Digital images of combined oceanic and continental data sets and their use in tectonic studies, EOS, AGU Trans., 64, 995-1004, 1983.

Mazzega P. and S. Houry, An experiment to invert Seasat altimetry for the Mediterranean and Black Sea mean surfaces, *Geophys. J. Int., 96*, 259-272, 1989.

Menke,W., Geophysical Data Analysis: Discrete Inverse Theory, *Academic Press Inc,* Orlando, Florida, 1984.

Moritz H., Least square collocation, Review of Geophys. and Space Phys:, 16, 421-430, 1978.

Parker R.L., The rapid calculation of potential anomalies, Geophys. J. R. astr. Soc., 31, 447-455, 1972.

Rapp, R.H., Detailed gravity anomalies and sea surface heights derived from geos-3/seasat altimeter data, Report n° 365 of the Dept of Geodetic Science and Surveying, The Ohio State University, 1985.

Ribe N.M. and A.B. Watts, The distribution of intraplate volcanism in the Pacific Ocean basin: a spectral approach, Geophys. J. R. astr. Soc., 71, 333-362, 1982.

Sandwell D.T., D.C. McAdoo and K.M. Marks, Antarctic Marine Gravity from Geosat and Seasat Altimetry, EOS trans. AGU, 71, 1643, 1990.

Tarantola, A., Inverse Problem Theory, Methods for Data Fitting and Model Parameter Estimation, Elsevier Science Publisher B. V. , Amsterdam, The Netherlands, 1987.

Vassiliou A.A. and K.P. Schwarz, Study of the High-frequency spectrum of the anomalous gravity potential, J. Geophys. Res., 92, 609-617, 1987.

N. Baudry, Seafloor Imaging Inc., BP 8039, Nouméa, New Caledonia.

S. Calmant, Orstom, BP A5, Nouméa, New Caledonia.

(Received December 5, 1990;
revised March 11, 1991;
accepted March 18, 1991.)